THE HYDROLYSIS OF HYDROXAMIC ACID COMPLEXANTS IN THE PRESENCE OF NON-OXIDISING METAL IONS 2: NEPTUNIUM (IV) IONS

F. P. L. Andrieux[a], C. Boxall[a*], I. May[b§], R. J. Taylor[c]

[a]Centre for Materials Science, University of Central Lancashire, Preston PR1 2HE, UK

[b]Centre for Radiochemistry Research, University of Manchester, Oxford Rd, Manchester M13 9PL

[c]Nexia Solutions Ltd, British Technology Centre, Sellafield, Seascale, Cumbria CA20 1PG, UK

*To whom all correspondence should be addressed. Centre for Materials Science, University of Central Lancashire, Preston PR1 2HE, UK. Tel.: +44 1772 893530; fax: +44 01772 892996. E-mail: cboxall@uclan.ac.uk

§ Current address: Inorganic, Isotope and Actinide Chemistry, (C-IIAC), Los Alamos National Laboratory, Mail Stop J-514, Los Alamos, NM 87545, U.S.A

Abstract

Hydroxamic acids are salt free, organic compounds with affinities for cations such as Fe^{3+}, Np^{4+} and Pu^{4+} and have been identified as suitable reagents for the control of Pu and Np in advanced nuclear fuel reprocessing. The results of a UV-visible-near IR spectrophotometric study of the 1:1 and 2:1 complexes formed between formo- and aceto- hydroxamic acids (FHA, AHA) and Np(IV) ions are interpreted using speciation diagrams for the identification of the species present at diferent pH and ligand to metal ratios. A kinetic model that describes the instability of the complex due to the hydrolysis of the hydroxamate moeity, previously developed for the Fe(III)-AHA complexes [1], is tested here against experimental Np(IV)-FHA data. Consequently, the complexation constant for formation of the 1:1 Np(IV)-FHA complex in nitric acid is estimated at $K_1 = 2715$, and indications are that complexation protects the ligand against hydrolysis at $0.1 > pH > -0.1$.

Keywords

Formohydroxamic acid, acetohydroxamic acid, Advanced Purex, neptunium, complexation, speciation, hydrolysis, kinetics.

1. Introduction

The separation and purification of uranium from neptunium and/or plutonium are major stages in the industrial scale reprocessing of spent nuclear fuel by the well known Purex process [2]. As described in our previous papers [3-6], the simple hydroxamic acids aceto- and formo- hydroxamic acids (AHA and FHA), where for AHA, R=CH_3 and for FHA, R=H, are salt free, hydrophilic organic compounds, RCONHOH, which act as bidentate O,O donor ligands and hence have high affinities for 'hard' cations such as Fe^{3+}, Np^{4+} and Pu^{4+}. These ligands, generically represented as XHA, are also redox active, electrochemical measurements having determined the onset potential for AHA oxidation on a gold electrode as +0.62 vs. saturated calomel electrode (SCE) at pH 1 [7]. We have previously studied the reduction of Np(VI) by FHA and Pu(IV) ions by FHA and AHA [8-9]. Chung has also reported on the reduction of Np(VI) by AHA [10]. These properties have led to them being identified as useful reagents for the control of Pu and Np in novel hydrometallurgical based actinide separation processes for Advanced Nuclear Fuel Cycles [3-5,11-12].

The kinetics of the acid hydrolysis of FHA and AHA in nitric acid to form hydroxylamine and the parent carboxylic acid have been determined [13] and are found, at $[HNO_3] < 3$ mol• dm^{-3} and when $[HNO_3] > [XHA]$, to obey Eq. (1).

$$-\frac{d[XHA]}{dt} = Ae^{-\frac{E_A}{RT}}[XHA][H^+] \qquad (1)$$

Where, for FHA and AHA respectively, A, the pre-exponential factor, is 9.09×10^9 and 3.22×10^9 $dm^3 \bullet mol^{-1} \bullet s^{-1}$ and E_A, the activation energy, is 77.3 and 79.9 $kJ \bullet mol^{-1}$. However, hydrolysis of hydroxamates bound to metal ions in a complex also occurs at different rates leading to the regeneration of the non-complexed metal ion in solution. It

has also been shown that the Pu(IV)-XHA complex is slowly reduced to free Pu(III) ions *via* the hydrolysis of the hydroxamate [9]. An understanding of these processes is vital if they are to be controlled within the design of any Advanced Purex process.

To this end, we have used UV-visible and near-IR electronic absorption spectrophotometry to experimentally study the kinetics of the hydrolysis of metal-XHA systems in nitrate media. Theoretical kinetic models have then been derived to interpret the experimental data. The models form two cases: (i) the metal ion complexes with, but does not oxidise the ligand (*i.e.* Fe^{3+}/AHA; Np^{4+}/FHA, Np^{4+}/AHA) and hydrolysis regenerates the free metal ion in solution; (ii) the metal ion both complexes and oxidises the ligand (Pu^{4+}/FHA; Pu^{4+}/AHA), thus reducing the metal ion. Our immediately previous paper [1] reports our findings with respect to the Fe(III)-AHA system as a prototypical example of the first class of system. This paper applies the kinetic model derived for Fe(III)-AHA to industrially relevant Np(IV)-AHA and Np(IV)-FHA systems, which behave analogously. The next paper in this series will extend the model to Pu(IV)-AHA complexes, an example of the second class of system.

2. Experimental Methods

2.1. Materials

Np(IV) aqueous stock was prepared using standard methods, which have been described previously [14], utilising stocks of NpO_2 held at Sellafield. Typical procedures followed were that, as required, gram quantities of the solid NpO_2 were dissolved by refluxing in strong HNO_3 in a radiochemical glovebox for several days until virtually complete

dissolution was obtained. Following Np and acidity analyses, the resultant solution would be decanted or filtered if required and diluted with HNO_3 to give a working stock solution. This would be sampled for acidity and Np analyses and checked spectrophotometrically for its valence purity. Np analysis was either by alpha spectrometry or low energy photon spectroscopy (LEPS) and the analytical results in Bq/ml converted to concentrations in mol•dm^{-3}; acidity was analysed in the standard manner by acid-base titrations with KF added to prevent Np hydrolysis. In such solutions, Np is present almost exclusively as Np(VI) with trace amounts of Np(V), the exact proportions dependent on factors including acidity and standing time. For this and related studies [14-15], Np stock solutions of 0.01 mol•dm^{-3} in 0.1 mol•dm^{-3} HNO_3 and 0.1 mol•dm^{-3} Np in 1.0 HNO_3 were prepared. Solutions of pure Np(IV) were obtained by reducing aliquots of the Np stock solution with substantial excess Fe(II) (as $FeCl_2$), diluted with HNO_3 such that the overall acidity was usually between 2-3 mol•dm^{-3} HNO_3. The resultant Np(IV) solution was purified from Fe and Cl ions by solvent extraction into 30% tributyl phosphate (TBP) in odourless kerosene (OK) and backwashing into 0.01 mol•dm^{-3} HNO_3. As the initial extraction extracted only 40-60 % of the Np(IV) the aqueous phase was often contacted with fresh TBP and the extracts combined. Backwashing, however, was efficient and required only a single contact. Extraction and stripping were carried out in centrifuge tubes using a motorised paddle stirrer at, usually, 1:1 solvent to aqueous ratios with mixing times of typically 10-15 minutes. Acid concentration would then be adjusted by addition of HNO_3 and the solution sampled for Np analysis. These procedures were used at different scales dependent on the number of planned experiments, specific conditions required and working limits in the fumehood. All solutions were made up accurately by volume. All

other reagents, including HNO_3 (70%, AnalaR, BDH Chemicals Ltd., Poole, Dorset, UK), AHA (Sigma-Aldrich Ltd, UK) and FHA (custom synthesis by Tocris Cookson Ltd, UK) were obtained from reputable suppliers at the highest available purity and used as received.

AHA and FHA were stored in a conventional refrigerator at 4 °C in order to prevent their decomposition. Solutions of FHA and AHA were prepared immediately prior to the experiments by room temperature dissolution of an accurately weighed portion in to distilled water to prevent hydroxamic acid hydrolysis.

2.2. Procedures

UV-visible-near infra-red (near IR) electronic absorption spectra (EAS) were recorded using a Perkin Elmer Lamda 19 spectrophotometer coupled by fibre optics to an external sample compartment for remote safe analysis of the α-active radioisotope ^{237}Np. Note that in the Figures the spectra have been offset for clearer comparisons.

Solutions for the kinetic experiments on Np(IV)-FHA complex stability were prepared by mixing aliquots of Np(IV) stock, HNO_3 and FHA directly into an optical cuvette (pathlength 1 cm). The complexant was added last. Solutions were mixed, stoppered and placed into the spectrophotometer whereupon data acquisition began immediately. During the kinetic absorbance measurements the spectrometer was set to scan the range 350 – 1000 nm at variable time intervals. Kinetic absorbance measurements were conducted over variable time periods up to a maximum of 900 minutes.

Some problems were encountered in these experiments with baseline shifts between experiments. This was probably an artefact of using remote analysis through long (10 m) fibre optics and, in some instances, inexact matrix matching in the reference beam. To correct for this, absorbances at two points on the baseline either side of the peak being monitored were taken and averaged. This gave an average baseline absorbance that can be subtracted from the peak absorbance to effectively correct for any baseline shifts. In generating the absorbance values used in the construction of Figs. 6 and 11, the Np(IV)-XHA complex peaks at 714 and 732 nm were corrected at 650 and 775 nm. Note also that the detector change at ~845 nm can distort the spectra in this region (e.g. Fig.4).

Caution: Np-237 is an emitter of alpha radiation and all experiments were carried out on the Sellafield nuclear licensed site in designated Controlled Areas under authorised specific procedures developed for working with Ionising Radiation.

3. Results and Discussion

3.1. Speciation and Kinetic Modelling of Metal-Hydroxamic Acid Systems

Previous work has shown that the Np(IV)-AHA system forms complexes with AHA:metal ratios from 1:1 to 3:1 [15]. Stability constants (β_1-β_3) for these Np(IV)-AHA complexes were obtained in non-complexing perchlorate media at a constant ionic strength. Unfortunately, the corresponding constants for the Np(IV)-FHA system were not determined as FHA is both less readily available (only through custom synthesis, vide supra) and is much less stable than AHA. However, the Np(IV)-FHA system is expected to behave in similar fashion to the Np(IV)-AHA system – consequently

interconversions between the free metal ion and complexes at 298 K for the latter system can be considered as being analogous to the former, where the equilibrium constants for the Np(IV)-AHA system in non-complexing perchlorate media are as follows [15]:

$$HL + Np^{4+} \xleftrightarrow{K_1} NpL^{3+} + H^+ \qquad K_1 = 2754 \qquad (2a)$$

$$HL + NpL^{3+} \xleftrightarrow{K_2} NpL_2^{2+} + H^+ \qquad K_2 = 5.49 \qquad (2b)$$

$$HL + NpL_2^{2+} \xleftrightarrow{K_3} NpL_3^{+} + H^+ \qquad K_3 = 4.47 \times 10^{-2} \qquad (2c)$$

Where HL = hydroxamic acid, L = hydroxamate anion.

From our earlier study of the Fe(III)-AHA system [1], it was found that the dynamics of the hydrolysis of the metal-AHA system in acid media such as HNO_3 and $HClO_4$ were complicated by metal-AHA complex speciation. Thus, in order to aid treatment of dynamic hydrolysis data obtained from the Np(IV)-XHA systems, initial speciation diagrams were calculated for the Np(IV)-AHA systems at 298 K as a function of [AHA] and pH - see Figs. 1-2, where pH = $-\log_{10}[H^+]$ and pHL = $-\log_{10}[AHA]$. The concentrations of individual species in both of these diagrams are given by:

$$[Np^{4+}] = \frac{M_T}{1 + K_1\gamma + K_2K_1\gamma^2 + K_3K_2K_1\gamma^3} \qquad (3a)$$

$$[NpL^{3+}] = K_1\gamma \frac{M_T}{1 + K_1\gamma + K_2K_1\gamma^2 + K_3K_2K_1\gamma^3} \qquad (3b)$$

$$[NpL_2^{2+}] = K_2K_1\gamma^2 \frac{M_T}{1 + K_1\gamma + K_2K_1\gamma^2 + K_3K_2K_1\gamma^3} \qquad (3c)$$

$$[NpL_3^{+}] = K_3K_2K_1\gamma^3 \frac{M_T}{1 + K_1\gamma + K_2K_1\gamma^2 + K_3K_2K_1\gamma^3} \qquad (3d)$$

$$\text{where } \gamma = \frac{[HL]}{[H^+]} = \frac{[NO_3^-]}{[H^+]} + \frac{L_T}{[H^+]} - 1 \quad (3e)$$

And L_T and M_T are the total concentrations of added Np(IV) (free or in complex) and AHA (free or in complex) respectively. It should be noted that Figs. 1-2 are calculated using the complexation constants of Eqs. (2a-2c) obtained in non-complexing perchlorate media. They do not allow for the weak complex formation that occurs between Np(IV) and NO_3^- *via* Eq. (4) in nitrate-containing media typical of reprocessing streams [16]. We shall return to this point shortly.

$$Np(NO_3)^{3+} \xleftrightarrow{K_D} NO_3^- + Np^{4+} \quad (4)$$

In our previous work on the Fe(III)-AHA system, a kinetic model was developed that described the hydrolysis of the Fe(III)-AHA complex. As both Fe(III) and Np(IV) do not oxidise the ligand, unlike Pu(IV) [9], their behaviour is analagous and we can assume that the mechanism developed in the Fe(III) case applies to the Np(IV)-XHA system [1]. For the purposes of deriving an analytical solution, we assume that the dominant form of the complex in the pH and pHL regions of interest is the mono-hydroxamato species ML. Experimentally, this requirement can be fulfilled by careful choice of reaction conditions using the speciation diagrams of Figs.1 & 2. Summarising the key points from the hydrolysis model developed in reference [1], the mechanism of hydrolysis follows Eq. (5-7).

$$HL + M \xleftrightarrow{K_1} C + H^+ \quad (5a)$$

$$HL + H^+ \xrightarrow{k_0} RCOOH + NH_3OH^+ \quad (5b)$$

$$C + mH^+ \xrightarrow{k_1} M + RCOOH + NH_3OH^+ \quad (5c)$$

$$\text{where } M_t = [Np^{4+}] \text{ at time t;} \quad (6a)$$

HL_t = [XHA] at time t; (6b)

C_t = [metal ion-XHA complex] at time t; (6c)

$k'_1 = k_1[H^+]^m$ assumed by analogy with (6d)

$k'_0 = k_0[H^+]$ in accordance with Eq. (1); and K_1 is given by: (6e)

The equilibrium described by K_1 is given by:

$$K_1 = \frac{C}{M\ HL}\lfloor H^+ \rfloor \quad (7)$$

The forward and back reactions associated with eqs. 2 are assumed to be fast on the timescale of XHA hydrolysis and so at equilibrium throughout the experiment. Further, given that the pK_a of both hydroxamic acids investigated in this study and subsequent papers in this series are greater than 8.5 (pK_a (FHA) = 8.78 [17]; pK_a (AHA) = 9.02 [18]), under the conditions employed in the experiments described below (pH < 1), the dominant form of the free ligand will be the acid rather than the deprotonated conjugate base. Thus, direct hydrolysis of the hydroxamate ion may be neglected. Mass balance on the metal cation, the ligand and nitrate anion at times t and t=0 demand that:

$HL_{T,0} = HL_0 + C_0$ $\qquad$ $HL_{T,t} = HL_t + C_t$ (8a,b)

$M_T = M_0 + C_0$ $\qquad$ $M_T = M_t + C_t$ (8c,d)

$[NO_3^-]_T = [NO_3^-] + MNO_3$ (8e)

where $[NO_3^-]_T$, MNO_3, $L_{T,t}$ and $L_{T,0}$ represent the total concentration of nitrate, concentration of metal ion-complexed nitrate (vide infra), total concentration of ligand (free or in complex) at time t and total concentration of ligand (free or in complex) at time t=0 respectively. Eq. 8b gives:

$$\frac{dHL_{T,t}}{dt} = \frac{dHL_t}{dt} + \frac{dC_t}{dt} \quad (9)$$

Similarly, eqs. 1, 6d and 6e give:

$$\frac{dHL_{T,t}}{dt} = k_0[H^+]HL_t + k_1[H^+]^m C_t = k'_0\, HL_t + k'_1\, C_t \quad (10)$$

Eqs. 7 and 8d give:

$$C_t = \frac{K'_1\, HL_t M_T}{[H^+] + K'_1\, HL_t} \quad (11)$$

$$\text{Where } K'_1 = \frac{K_1}{1 + ([NO_3^-]_T / K_D)} \quad (12)$$

for nitrate-complexing actinide(IV) species. The parameter K_D describes the dissociation of the weak complex formed between e.g. Np(IV) and NO_3^- via eq. 4. Differentiation of eq. 11 and substitution into eq. 9 gives:

$$\frac{dHL_{T,t}}{dt} = \frac{dHL_t}{dt}\left(1 + \frac{K'_1[H^+]M_T}{\left([H^+] + K'_1\, HL_t\right)^2}\right) \quad (13)$$

Substitution of eq. 11 into 10 and substituting the result into eq. 13 then gives:

$$\frac{dHL_t}{dt} = -HL_t \frac{\left(k'_0 + \frac{k'_1 K'_1 M_T}{[H^+] + K'_1\, HL_t}\right)}{\left(1 + \frac{K'_1[H^+]M_T}{\left([H^+] + K'_1\, HL_t\right)^2}\right)} \quad (14)$$

Full solution of eq. 14 gives:

$$t = \frac{1}{k'_1}\ln\left(\frac{\frac{K'_1 HL_t}{[H^+]}+1}{\frac{K'_1 HL_0}{[H^+]}+1}\right) - \left(\frac{\frac{K'_1 M_T}{[H^+]}+1}{\frac{k'_1 K'_1 M_T}{[H^+]}+k'_0}\right)\ln\left(\frac{HL_t}{HL_0}\right) - \left(\frac{\frac{k'^2_1 K'_1 M_T}{[H^+]}+k'^2_0}{\frac{k'_0 k'^2_1 K'_1 M_T}{[H^+]}+k'^2_0\, k'_1}\right)\ln\left(\frac{\frac{K'_1 HL_t}{[H^+]}+1+\frac{k'_1 K'_1 M_T}{k'_0[H^+]}}{\frac{K'_1 HL_0}{[H^+]}+1+\frac{k'_1 K'_1 M_T}{k'_0[H^+]}}\right) \quad (15)$$

where HL_0 may be obtained by solving the quadratic produced by substitution of eq. 11 into eq. 8a at t=0. Eq. 15 is insoluble with respect to HL_t. However, it can be used to

calculate theoretical HL_t *vs* t and, through eq. 11, C_t *vs* t plots. Curve fitting these to experimental data allows for the extraction of values of key parameters such as $k'_1 = k_1[H^+]^m$ as a function of $[H^+]$. A plot of $\log_{10} (k_1[H^+]^m)$ *vs* $\log[H^+]$ then allows calculation of values of m and k_1.

Curve fitting of experimental C_t *vs* t plots through use of eqs. 11 and 15 is facilitated by the observation of k_1 and K'_1 having different effects on the shape of the calculated C_t vs t curve. These effects are illustrated in Fig.3 and may be qualitatively understood as follows. The rate parameter k_1 affects the overall duration of the decrease in concentration of complex with time, although this effect is found to vanish for very small values of k_1. This is readily understood in that once the process associated with k_1 (eq. 5c) is much slower than the parallel process associated with k_0 (eq. 5b) (i.e. $k_1[H^+]^m << k_0[H^+]$), the latter process determines the overall rate. In contrast, no matter the overall duration of the decay in complex concentration, the equilibrium constant K'_1 only affects the degree of sigmoid character in the C_t vs t profile with a pseudo-induction period appearing at large K'_1 during which C_t is invariant with time. The larger K'_1 at any one set of otherwise constant experimental conditions, the longer the induction period before the concentration starts to decay. Again, this may be readily understood in that the larger K'_1, the longer a significant / measurable concentration of complex will maintain during the overall decay time.

3.2. Experimental Studies of the Np(IV)-AHA & Np(IV)-FHA Systems

Section 3.1 described how the derivation of the kinetic model for AHA hydrolysis when bound to Np(IV) ions using available complexation constants. This section will present EAS data for the Np(IV)-AHA system and show how it can be understood in terms of

the speciation diagrams. By comparing EAS for Np(IV)-AHA and Np(IV)-FHA systems we can then justify the application of the kinetic model to the Np(IV)-FHA hydrolysis data where complexation constants are not available and must be estimated during the data processing.

Near IR spectroscopy is a well established technique for monitoring Np oxidation states in solution [19-20]. Fig. 4 shows a Np(IV) spectrum in 0.1 mol•dm^{-3} HNO_3 in the presence of AHA at L:M ratios of 0:1 to 4.85:1. It can be seen that, in the presence of AHA, the spectrum is still characteristic of Np(IV) although the peak shapes have changed notably. This contrasts with U(VI) and Pu(IV) AHA complexes where strong colour changes and very different EAS are observed [13,21]. Comparison with Fig. 1 reveals that the spectrum obtained at an AHA:Np(IV) ratio of 0.97:1 (pHL = 2.31) was recorded under conditions where the $Np(AHA)^{3+}$ complex comprises 90% of all Np(IV) present. A similar analysis of the spectrum obtained at an AHA:Np(IV) ratio of 4.85:1 (pHL = 1.61) indicates that it was recorded under conditions where the $Np(AHA)^{3+}$ and $Np(AHA)_2^{2+}$complexes comprise 53 and 47 % respectively of all Np(IV) present. Apart from minor variations the absorption spectra recorded at low and high total AHA concentration are quite similar, implying a resemblance between the near IR spectra of the 1:1 and 2:1 AHA-Np(IV) complexes. (It is worth noting at this point that use of Fig. 1 as an aid to the analysis of Fig 4 should usually be conducted with caution. Fig. 1 was generated using Np(IV)-AHA complexation constants recorded in non-complexing perchlorate media whilst the data of Fig. 4 was recorded in nitrate media, NO_3^- forming a weak complex with Np(IV) that dissociates in accordance with eq. 4. However, when this weak complexation is explicitly accounted for in the speciation diagram, as in Fig. 8 below, it is found that it has virtually no effect on the speciation of the $Np(AHA)^{3+}$

and $Np(AHA)_2^{2+}$complexes in the pHL range studied in Fig. 4 – thus those conclusions drawn as a result of the comparison of Fig. 4 with Fig. 1 are valid.)

The resemblance between the near IR spectra of the 1:1 and 2:1 AHA-Np(IV) complexes is further highlighted by Fig. 5 which presents the absorbance spectra of a solution of 0.005 mol•dm^{-3} Np(IV), 0.1 mol•dm^{-3} AHA (L:M = 20:1), recorded in the pH range 0.8 to –0.6. Fig. 2 indicates that, at the lower end of this pH range at e.g. pH –0.3, $Np(AHA)^{3+}$ is the dominant species in solution while at higher pHs e.g. pH 0.8, $Np(AHA)_2^{2+}$ dominates. The broad similarities between these two spectra indicate that the spectral features of the mono-acetohydoxamato and di-acetohydroxamato complexes are near co-incident and so difficult to deconvolute. (It is again worth noting that Fig. 2 was generated using Np(IV)-AHA complexation data recorded in non-complexing perchlorate whilst the data of Fig. 5 was recorded in nitrate media. However, when complexation of Np(IV) with nitrate is again explicitly accounted for, as in Fig. 9 below, it is found that it has no effect on the nature of the most dominant species at the pHs selected for the comparison of their spectra – specifically pHs 0.8 and –0.3. Thus, the conclusions drawn as a result of the comparison of Fig. 5 with Fig. 2 are valid.)

From Fig. 5 it can be seen that the shapes of two of the main peaks at 714 and 732 nm remain largely unchanged up to 1 mol•dm^{-3} HNO_3. Fig. 6 then shows the absorbance at 714 and 732 nm of a solution of 2.5 x 10^{-3} mol• dm^{-3} Np(IV) and 0.05 mol• dm^{-3} AHA as a function of [HNO_3] in the range 0.1 to 4 mol•dm^{-3} (pH 1 to –0.6). Inspection of the speciation diagram shown in Fig. 2 leads us to expect that the dominant species are the $Np(AHA)^{3+}$ and $Np(AHA)_2^{2+}$ complexes, although this expectation should again be treated with caution given that Fig. 2 was calculated for perchlorate media at total

Np(IV) and AHA concentrations double those used in the experiment of Fig. 6. Due to the coincidence of the absorption spectra in the 700-750 nm region noted above, we assume that the absorbances at 714 and 732 nm are compound entities, both being directly proportional to ($[Np(AHA)^{3+}] + [Np(AHA)_2^{2+}]$). We shall return to the validity of this assumption shortly. Fig. 6 then shows the fitting of calculated values of ($[Np(AHA)^{3+}] + [Np(AHA)_2^{2+}]$) as a function of $[HNO_3]$ to experimental absorbance data. The calculated values of $[Np(AHA)^{3+}]$ and $[Np(AHA)_2^{2+}]$ were obtained by use of eqs. 16b and 16c. Eqs. 16 were produced by modification of eqs. 3 to account for the weak complexation of Np(IV) with nitrate.

$$[Np^{4+}] = \frac{M_T}{\left(\frac{4M_T + [HNO_3]}{K_D}\right) + 1 + K_1\gamma + K_2K_1\gamma^2 + K_3K_2K_1\gamma^3} \quad (16a)$$

$$[NpL^{3+}] = \frac{K_1\gamma\, M_T}{\left(\frac{4M_T + [HNO_3]}{K_D}\right) + 1 + K_1\gamma + K_2K_1\gamma^2 + K_3K_2K_1\gamma^3} \quad (16b)$$

$$[NpL_2^{2+}] = \frac{K_2K_1\gamma^2\, M_T}{\left(\frac{4M_T + [HNO_3]}{K_D}\right) + 1 + K_1\gamma + K_2K_1\gamma^2 + K_3K_2K_1\gamma^3} \quad (16c)$$

$$[NpL_3^{+}] = \frac{K_3K_2K_1\gamma^3\, M_T}{\left(\frac{4M_T + [HNO_3]}{K_D}\right) + 1 + K_1\gamma + K_2K_1\gamma^2 + K_3K_2K_1\gamma^3} \quad (16d)$$

where $[HNO_3]$ is the nominal concentration of added nitric acid and K_D, which is defined by eq. 4, is used as a fitting parameter. K_1, K_2 and K_3 are as given in eq. 2.

The illustrated fit to the experimental data in Fig. 5 was calculated using $K_D = 0.15$. Considering the assumptions made in this data fitting and the inherent difficulties in measuring equilibrium constants for weak bases of strong acids, this value is in good

agreement with the accepted literature value of 0.46 (range 0.58-0.36) calculated from $\log_{10}K_1 = 0.34 \pm 0.10$, which was determined in 1 M $HClO_4$ at 20 °C by Danesi and co-workers [16,20].

The derived value of K_D can then be used to produce a speciation diagram, Fig. 7, calculated as a function of pH for the experimental conditions employed in Fig. 6. Inspection of Fig.7 indicates that the dominant species over the range of acidities used in Fig. 6 are the $Np(AHA)^{3+}$ and $Np(AHA)_2^{2+}$ complexes, which together comprise >95% of all Np(IV) at [H+] < 1 mol•dm^{-3} and >70% at [H+] < 4 mol•dm^{-3}. This observation, together with the value of K_D obtained from the curve fitting exercise of Fig. 6, validates our earlier assumption that the absorbances at 714 and 732 nm are compound entities, both being directly proportional to ($[Np(AHA)^{3+}] + [Np(AHA)_2^{2+}]$).

Experimental derivation of a value for $K_D = 0.15$ now allows for Figs. 1-2 to be recalculated using eqs. 16 and Np(IV)-AHA complexation constants as given in Eq. (2a-c). The resultant speciation diagrams for the Np(IV)-AHA system, which allow for nitrato complex formation, are shown in Figs. 8-9.

From Eq. (1), the half lives for the acid catalysed hydrolysis of free FHA and AHA in 1 mol•dm^{-3} HNO_3 at 293 K are 1¼ and 10½ hours respectively The half lives for both ligands are less at higher acidities. The parameters k'_1 and K'_1 for the hydrolysis of bound XHA can be obtained from kinetic absorbance experiments by curve fitting normalised absorbance *vs* t plots using Eqs. (11 & 15). However, use of these equations requires the availability of an accurate and reliable value of k'_0, the rate parameter describing the kinetics of the hydrolysis of the free ligand. It is widely held that the mechanism underpinning the description of k'_0 given by Eq. (1) involves [22]:

(i) rapid pre-equilibrium protonation of the carbonyl oxygen; followed by,

(ii) nucleophilic attack by water at the carbonyl carbon, resulting in the formation of a tetrahedral intermediate; followed by,

(iii) re-creation of carbonyl at the new tetrahedral C with loss of a hydroxylamine leaving group (NH_2OH).

However, at $[HNO_3] > 3$ mol•dm^{-3}, there is a possibility of a departure from this mechanism and so the validity of Eq. (1) [22], thus making use of Eq. (11 & 15) difficult at high acidities. Thus, even though the complexation constants for the Np(IV)-FHA system are unknown, it was decided that it would be both expeditious and appropriate to first study the effect of Np(IV) complexation on the hydrolysis of FHA at intermediate pH (pH > -0.1) rather than AHA at higher $[H^+]$ with its attendant risk of a mechanism change.

Absorption spectra of the Np(IV)-FHA system are given in Fig. 10, recorded as a function of nitric acid concentration, 0.1-3 mol• dm^{-3}. There are broad similarities with the Np(IV)-AHA spectra shown in Fig. 5; major peaks differ only by 1-2 nm. However, there are some subtle differences. The absolute intensities of the absorbance features across the wavelength ranges studied are lower for the Np(IV)-FHA system than Np(IV)-AHA. The 723 nm $Np(IV)_{aq}$ peak appears to remain in the spectra; the 975 nm peak decreases in intensity with increasing HNO_3 and the 954 nm satellite peak is only clearly discernible in the intermediate spectra (0.40 and 1.01 M HNO_3).

These spectra suggest that whilst isostructural complexes are formed, complexation is somewhat weaker with FHA than with AHA. It seems likely therefore that, as with AHA, the absorbances at 714 nm and 732 nm may be treated as compound entities

whose intensities are directly proportional to ([$Np(FHA)^{3+}$] + [$Np(FHA)_2^{2+}$]). The time dependence of the absorbance data recorded from Np(IV)-FHA systems at two nitric acid concentrations are shown in Fig. 11. Differences in the absorbance values at t=0 are due to the differences in complex speciation between the two pHs studied.

The data of Fig. 11 can be analysed by use of Eqs. (11 & 15). However, these equations make no allowance for the formation of $Np(FHA)_2^{2+}$, although, as noted above, overall complexation in the Np(IV)-FHA system is weaker than in the Np(IV)-AHA. A recalculation of Fig. 9 (not shown) based on this observation indicates that, in the pH region of the measurements shown in Fig. 11, $Np(FHA)_2^{2+}$ accounts for only ~15% of the total concentration of Np species. This suggests that it is a reasonable approximation to assume that the contribution made by Np(IV)-FHA complexes to the absorbance data of Fig. 11 is derived mainly from the $Np(FHA)^{3+}$ species. Eq. (15) is then be applicable to the data of Fig. 11.

Curve-fitting the data of Fig. 11 to Eq. (11 & 15) is now relatively straightforward but involves a number of steps as follows:

(i) the generation of a [$Np(FHA)^{3+}$] or C_t vs t curve using eq 15 (producing a t vs HL_t plot) in conjunction with eq 11 (generating a C_t vs t plot from the aforementioned t vs HL_t plot);

(ii) from the so-generated C_t vs t plot and the mass balance of eq. 8d, generation of an uncomplexed [metal ion] or M_t vs t plot;

(iii) the conversion of both C_t vs t and M_t vs t plots to absorbance vs t plots;

(iv) the combining of the complex and metal ion absorbance vs t plots to give an overall absorbance vs t plot; and finally

(v) the fitting of the overall absorbance vs t plot to the experimental data of Fig. 11 by use of K'_1 and k'_1 as fitting parameters in eq. 15 (see Figs. 3, vide supra).

Step (iii) in this process requires the availability of extinction coefficients for both $Np(FHA)^{3+}$ and the non FHA-complexed metal ion. The former can be obtained from the measured absorption at long time for the absorbance vs t plot at $[HNO_3]$ = 1.3 $mol \bullet dm^{-3}$ in Fig. 10. At this point, the model of eq. 5 suggests that all FHA has been hydrolysed and that absorbance is due entirely to uncomplexed Np, [Np(IV)] = 0.005 $mol \bullet dm^{-3}$. This is supported by the fact that, at this acidity, the measured absorbance is invariant with t at t > 35000 s. As the measured absorbance asymptotically approaches 0.15 at long t, and given that a 1 cm cell was used in all measurements, an extinction coefficient for the non-FHA complexed metal ion of 30 $dm^3 \bullet mol^{-1} \bullet cm^{-1}$ can be obtained. In-house measurements of the UV-visible and near-IR spectrum of Np(IV) as a function of $[HNO_3]$ (not shown) indicate that the absorbance at the wavelength employed in Fig. 11, λ = 732 nm, is near invariant with nitric acid concentration around $[HNO_3]$ = 1 $mol \bullet dm^{-3}$. Thus, the value of the extinction coefficient for non-FHA complexed Np(IV) derived at $[HNO_3]$ = 1.3 $mol \bullet dm^{-3}$ can also be used in the interpretation of the data recorded at $[HNO_3]$ = 0.79 $mol \bullet dm^{-3}$.

Measured absorbance at t = 0 in Fig. 11 is greater at $[HNO_3]$ = 0.79 $mol \bullet dm^{-3}$ than at $[HNO_3]$ = 1.3 $mol \bullet dm^{-3}$ suggesting, as would be expected, that the concentration of FHA-complexed Np(IV) is greater at the lower acidity. If it is assumed that all Np(IV)

is complexed with FHA at t = 0 at [HNO_3] = 0.79 mol•dm^{-3} then the measured absorbance of 0.337 allows calculation of an extinction coefficient for FHA-complexed Np(IV) of 67.4 dm^3•mol^{-1}•cm^{-1}. Interestingly, the measured absorbance of $Np(FHA)^{3+}$ at 732 nm as a function of [HNO_3] in a Np(IV)-FHA system comprised of 0.0025 Np(IV) mol•dm^{-3} and 0.05 mol•dm^{-3} FHA (not shown) exhibits a maximum saturation value of 0.17 at [HNO_3] < 1 mol•dm^{-3}. This suggests that all Np(IV) is complexed with FHA, so allowing calculation of a value of the extinction coefficient of 68 dm^3•mol^{-1}•cm^{-1}, in excellent agreement with the value calculated from Fig. 11.

Thus, use of extinction coefficient values of 30 and 68 dm^3•mol^{-1}•cm^{-1} for non-FHA complexed and FHA complexed Np(IV) respectively then allows for the execution of steps (iii) to (v) above. As discussed in reference to Fig. 3 above, step (v) is facilitated by the fact that only two parameters are unknown for the Np(IV)-FHA system: K'_1 and k'_1, each parameter having a different effect on the shape of the calculated [$Np(FHA)^{3+}$] *vs* time curve, so simplifying the fitting process (Fig. 3). Bearing this qualitative interpretation in mind, the results of using Eq. (11), (15) and (8d) to curve fit the data of Fig. 11 are shown in Fig. 12 and 13 for [HNO_3] = 0.79 and 1.3 mol•dm^{-3} respectively. Both Figs. 12 and 13 shown separate calculated absorbance vs t plots for the non-FHA complexed metal ion and FHA complexed metal ion as well as the calculated compound absorbance for both species. It is the latter that is fitted to the experimental data, also shown in each figure, with the following results.

The parameter k'_1 is found to be less than 7.9 x 10^{-6} and 1.3 x 10^{-5} s^{-1} at 0.79 and 1.3 mol•dm^{-3} nitric acid concentrations respectively. Use of lower values than this leads to no significant change in the calculated [$Np(FHA)^{3+}$] *vs* time profiles, whilst larger

values lead to a significant decrease in the quality of fit, no matter the value of K'_1 employed. Comparison of these values of k'_1 with k'_0 under the same conditions (1.19 x 10^{-4} and 1.96 x 10^{-4} s^{-1} respectively) suggests that, over the range of acidities studied in Fig. 11, complexation of FHA with Np(IV) actually protects the ligand against acid catalysed hydrolysis.

This result is in contrast to results observed from the Fe(III)-AHA system [1] which suggests that complexation with Fe^{3+}accelerates the rate of hydrolysis of AHA. This can perhaps be qualitatively understood through the observation that in the Fe(III)-AHA system a proton in the rate determining step interacts with a dipositive FeL^{2+} complex. If it is assumed that analogous mechanisms to the Fe(III)-AHA system operate in the Np(IV)-FHA system, the complex would initially have a 3+ charge, NpL^{3+}, so rendering the interaction with a proton more unfavourable compared to the Fe(III)-AHA system.

K'_1 is found to have values of 431 and 280 at 0.79 and 1.30 mol•dm^{-3} nitric acid concentrations respectively. Simultaneous solution of Eq. (12) at each concentration allows the extraction of values of K_D and K_1 of 0.15 and 2715 respectively. This value of K_D derived from the Np(IV)-FHA kinetic data of Fig. 11 is in excellent agreement with the value of 0.15 derived from the Np(IV)-AHA speciation data of Figs 6 and 7. The derived value of K_1 for the Np(IV)-FHA system also confirms the suggestion made from the absorption spectra that complexation of Np(IV) by FHA is weaker than with AHA, where the analogous parameter has a value of 2754 ((Eq. (2a)). This is consistent with the pK_a for FHA being less than that for AHA, 8.78 and 9.02 respectively [17-18], leading to the expectation that FHA will form less strong complexes with metal ions. Qualitatively, the difference in both pK_a and K_1 values for FHA and AHA can be

understood by noting that the methyl substituent on the CO group in AHA will exert a stronger electron-donating inductive effect than the corresponding H atom in FHA.

A comparison of the theoretical total absorbance *vs* time profiles with the experimentally measured total absorbanc vs t plots of Fig. 11 are shown in Figs. 12 and 13. The excellent agreement further supports our assumption that, under the experimental conditions employed in Fig. 11, the absorbance measured at 732 nm is, in the first approximation, nearly entirely due to the $Np(FHA)^{3+}$ species.

4. Conclusions

Np(IV) readily complexes with both FHA and AHA in dilute nitric acid. This can be observed by Np(IV) peak changes in the near IR region. The spectra of the 1:1 and 2:1 XHA-Np(IV) complexes bear a strong resemblance to each other making spectral de-convolution a non-trivial exercise. However, with the aid of speciation diagrams, Np(IV) absorption spectra in the presence of AHA and FHA have been interpreted and experimental conditions have been identified under which the 1:1 FHA-Np(IV) complex can be assumed to be the majority species.

Secondly, by application of a kinetic model derived for the analogous Fe(III)-AHA system, spectrophotometric studies of the acid-catalysed hydrolysis of FHA while bound to Np(IV) have been modelled and explained. This kinetic analysis also allows for the calculation of the first complexation constant for the Np(IV)-FHA system, with K_1 being found to have a value of 2715. Complexation by Np(IV) in the form of the 1:1 complex protects FHA against acid-catalysed hydrolysis and has useful implications for

the applications of XHAs in the reprocessing of irradiated nuclear fuel. In the context of an Advanced Purex process, the robustness of the associated process flow sheet would be favourably enhanced by such protection. However, this work has focused on using example data to validate that the kinetic model can be applied to Np(IV) and estimating K_1 and k_1' for the Np(IV)-FHA system. It now needs to be applied to a broader range of ligand and nitric acid concentrations for both FHA and AHA to better refine the complexation and reaction rate parameters. Subsequent extension of these modelling approaches to Pu(IV) ions would then provide a sound basis to fully understand the stability of hydroxamic acids and their actinide complexes in process flow sheets. This will be the subject of our next communication.

Acknowledgements

The authors wish to thank British Nuclear Fuels Ltd and the Nuclear Decommissioning Authority (NDA) for financial support and for a post-doctoral research fellowship for FA. This paper is based in part on work that was first published in a preliminary form in the Proceedings of Actinides 2005 [23].

References

[1] Andrieux, F.P.L., Boxall, C., Taylor, R.J.: The Hydrolysis of Hydroxamic Acid Complexants in the Presence of Non-Oxidising Metal Ions 1: Ferric Ions. J. Solution Chem. in press (2007).

[2] Dennis, I.S., Jeapes, A.P., Reprocessing Irradiated Fuel. In: Wilson, P.D., Ed., The Nuclear Fuel Cycle, Oxford Science Publications, Chapter 7, p.116, 1996.

[3] Birkett, J.E., Carrott, M.J., Fox, O.D., Jones, C.J., Maher, C.J., Roube, C.V., Taylor, R.J., Woodhead, D.A.: Recent Developments in the Purex Process for Nuclear Fuel Reprocessing: Complexant Based Stripping for Uranium - Plutonium Separation. Chimia 59, 898-904 (2005).

[4] Taylor, R.J., May, I., Wallwork, A.L., Dennis, I.S., Hill, N.J., Galkin, B.Y., Zilberman, B.Y., Fedorov, Y.S.: The Applications of Formo- and Aceto-Hydroxamic Acids in Nuclear Fuel Reprocessing. J.Alloys Comp. 271-273, 534-537 (1998).

[5] Birkett, J.E., Carrott, M.J., Fox, O.D., Jones, C.J., Maher, C.J., Roube, C.V., Taylor, R.J., Woodhead, D.A.: Controlling Neptunium and Plutonium within Single Cycle Solvent Extraction Flowsheets for Advanced Fuel Cycles. J. Nucl. Sci. Tech. 44, 337-343 (2007).

[6] Taylor, R.J.: Progress towards understanding the interactions between hydroxamic acids and actinide ions. J. Nucl. Sci. Tech., Supp. 3, 886-889 (2002).

[7] Shackleford, S.; Development of an EQCM-based Sensor for Metal Ions, PhD Thesis, University of Central Lancashire (2002).

[8] Colston, B.J.; Choppin, G.R.; Taylor, R.J. A preliminary study of the reduction of Np(VI) by formohydroxamic acid using stopped-flow near-infrared spectrophotometry. Radiochimica Acta 88, 329-334 (2000).

[9] Taylor, R.J., Mason, C., Cooke, R., Boxall, C.: The Reduction of Pu(IV) by Formohydroxamic Acid in Nitric Acid. J.Nucl.Sci.Tech. Supplement 3, 278-281 (2002).

[10] Chung, D.Y., Lee, E.H.: The reduction of Np(VI) by acetohydroxamic acid in nitric acid solution. In *Recent Advances In Actinide Science*; Alvarez, R., Bryan, N.D., May, I., Eds.; Royal Society of Chemistry, Cambridge, 587-589 (2006).

[11] Fox, O.D., Jones, C.J., Birkett, J.E., Carrott, M.J., Maher, C.J., Roube, C.V. Taylor, R.J.: Advanced PUREX flowsheets for future Np and Pu fuel cycle demands. In: Separations for the Nuclear Fuel Cycle in the 21st Century; Lumetta, G.J, Nash, K.L., Clark, S.B., Friese, J.I., Eds. ACS Symposium Series 933, ACS, Washington DC. USA, 89-102, 2006.

[12] Todd, T.A., Wigelund, R.A., Advanced Separation Technologies for Processing Spent Nuclear Fuel and the Potential Benefits to a Geologic Repository. In: Separations for the Nuclear Fuel Cycle in the 21st Century; Lumetta, G.J, Nash, K.L., Clark, S.B., Friese, J.I., Eds. ACS Symposium Series 933, ACS, Washington DC. USA, 41-56, 2006.

[13] Taylor, R.J., May, I.: The Reduction Of actinide ions by hydroxamic acids, Czech J. Phys., 49, 617-621 (1999).

[14] May, I., Taylor, R.J., Brown, G., Hill, N.J.: Np(IV) distribution between 30% tributyl phosphate in odourless kerosene and nitric acid. Radiochim. Acta 83, 135-138 (1998).

[15] Taylor, R.J., Sinkov, S.I., Choppin, G.R., May, I.: Solvent Extraction Behaviour of Neptunium Ions in the Presence of Simple Hydroxamic Acids, Solvent Extraction and Ion Exchange, under review (2007).

[16] Danesi, P.R., Chiarizia, R., Scibona, G., D'Alessandro, G.: Stablity constants of nitrate and chloride complexes of Np(IV), Np(V) and Np(VI) ions. J. Inorg. Nucl. Che. 33, 3502-3510 (1971).

[17] Phillips, R.J.: Chelating ion exchange with macrorecticular hydroxamic acid resins, Ph.D. Thesis, Iowa State University, IS-T-910 (1980).

[18] Monzyk, B., Crumbliss, A.L.: Acid dissociation constants (Ka) and their temperature dependencies (ΔHa, ΔSa) for a series of carbon- and nitrogen-substituted hydroxamic acids in aqueous solution. J. Org. Chem. 45, 4670-4675 (1980).

[19] Friedman, H.A., Toth, L.M.: Absorption spectra of Np(III), (IV), (V) and (VI) in nitric acid solution, J. Inorg. Nucl. Chem., 42, 1347-1349 (1980).

[20] Yoshida, Z., Johnson, S.G., Kimura, T., Krsul, J.R., Neptunium, in The chemistry of the actinide and transactinide elements, 3rd ed. Eds. L.R. Morss, N.M. Edelstein, J. Fuger, Springer, Netherlands (2006).

[21] May, I., Taylor, R.J., Denniss, I.S., Brown, G., Wallwork, A.L., Hill, N.J., Rawson, J.M., Less, R.: Neptunium(IV) and Uranium(VI) Complexation by Hydroxamic Acids. J. Alloys Cpds. 275-277, 769-772 (1998).

[22] Ghosh, K.K.: Kinetic and Mechanistic Aspects of Acid Catalysed Hydrolysis of Hydroxamic Acids. Indian J.Chem. 36B, 1089-1102 (1997).

[23] Taylor, R.J., Boxall, C., Andrieux, F., Mason, C.: Modelling the hydrolysis of Actinide complexed Hydroxamic Acid Ligands. In: May, I., Alvarez, R., Bryan, N., Eds., Recent Advances in Actinide Science The Royal Society of Chemistry, Cambridge, pp.626-628, 2006.

Figure Captions

Figure 1. Speciation diagram for Np^{4+} - AHA system at 298 K showing concentrations of Np^{4+}, NpL^{3+}, NpL_2^{2+} and NpL_3^{+} (data series 1-4 respectively) as functions of total AHA concentration (expressed as pHL) calculated at total [Np(IV)] = 0.005 mol•dm^{-3} and [HNO_3] = 0.1 mol•dm^{-3}, pH=1.

Figure 2. Speciation diagram for Np^{4+} - AHA system at 298 K showing concentrations of Np^{4+}, NpL^{3+}, NpL_2^{2+} and NpL_3^{+} (data series 1-4 respectively) as functions of pH calculated at total [Np(IV)] = 0.005 mol•dm^{-3} and total [AHA] = 0.1 mol•dm^{-3}, pHL=1, corresponding to AHA:Np ratio of 20:1.

Figure 3. Normalised C_t vs t calculated using eqs. 15 and 11. All data series calculated for AHA using M_T = 0.005 mol•dm^{-3}, HL_T = 0.1 mol•dm^{-3}, pH = 0, k_0 = 1.836 x 10^{-5} dm^3•mol^{-1}•s^{-1} and m=1. (a) k_1 = 2 x 10^{-3} dm^6•mol^{-2}•s^{-1}, data series 1-4 corresponding to K'_1 = 25, 100, 250, 1000 respectively. (b) K'_1 = 250, data series 1-6 corresponding to k_1 = 1 x 10^{-3}, 5 x 10^{-4}, 2.5 x 10^{-4}, 1 x 10^{-4}, 1 x 10^{-5}, 1 x 10^{-6} dm^6•mol^{-2}•s^{-1} respectively.

Figure 4. Near IR spectra of 0.005 mol•dm^{-3} Np(IV) in 0.1 mol•dm^{-3} HNO_3 in presence of 0, 0.0049 (ligand:Np(IV) ratio = 0.97:1), 0.0097 (ratio = 1.93:1), 0.0218 (ratio = 4.35:1) and 0.0243 (ratio = 4.85:1) mol•dm^{-3} AHA

Figure 5. Near IR spectra of 0.005 mol•dm^{-3} Np(IV) in 0.1 mol•dm^{-3} AHA in the presence of 0.15, 0.68, 1.22, 2.03, 2.93 and 3.76 mol•dm^{-3} HNO_3 (pH = 0.8 to –0.6).

Figure 6. Plot of normalised absorbance of Np(IV)-AHA system at 732 nm (series 2) and 714 nm (series 3) as functions of [HNO_3]. Total Np(IV) and AHA concentrations =

2.5 x 10^{-3} and 0.05 mol•dm^{-3} respectively. Series 1 shows normalised ([$Np(AHA)^{3+}$] + [$Np(AHA)_2^{2+}$]) as a function of [HNO_3], calculated using Np(IV)-AHA complexation constants as given in Eq. (2a-e) and K_D = 0.15.

Figure 7. Speciation diagram for Np^{4+} - AHA system at 298 K showing concentrations of $Np(NO_3)^{3+}$, Np^{4+}, NpL^{3+}, NpL_2^{2+} and NpL_3^{+} (data series 1-5 respectively) as functions of pH calculated at total Np concentration of 2.5 x 10^{-3} mol•dm^{-3} and total [AHA] = 0.05 mol•dm^{-3}, pHL=1.3, corresponding to AHA:Np ratios of 20:1.

Figure 8. Speciation diagram for Np^{4+} - AHA system at 298 K showing concentrations of $Np(NO_3)^{3+}$, Np^{4+}, NpL^{3+}, NpL_2^{2+} and NpL_3^{+} (data series 1-5 respectively) as functions of total AHA concentration (expressed as pHL) calculated at total Np concentration of 0.005 mol•dm^{-3} and [HNO_3] = 0.1 mol•dm^{-3}, pH=1.

Figure 9. Speciation diagram for Np^{4+} - AHA system at 298 K showing concentrations of $Np(NO_3)^{3+}$, Np^{4+}, NpL^{3+}, NpL_2^{2+} and NpL_3^{+} (data series 1-5 respectively) as functions of pH calculated at total [Np(IV)] = 0.005•mol dm^{-3} and total [AHA] = 0.1 mol•dm^{-3}, pHL=1, corresponding to AHA:Np ratios of 20:1.

Figure 10. Near IR spectra of 0.005 mol•dm^{-3} Np(IV) in 0.1 mol•dm^{-3} FHA in the presence of 0.15, 0.40, 1.01 and 2.88 mol•dm^{-3} HNO_3 (pH = 0.8 to –0.5).

Figure 11. Absorbance of mixture of 0.005 mol•dm^{-3} Np^{4+} and 0.1 mol•dm^{-3} FHA (total FHA:Np(IV) ratio = 20:1) measured at 293 K at λ = 732 nm as function of time. Experiments conducted in nitric acid solutions wherein [HNO_3] = 0.79 and 1.3 mol•dm^{-3} as indicated in legend.

Figure 12. Experimental and theoretical absorbance vs t plots for the Np(IV)-FHA system at [HNO_3] = 0.79 mol•dm^{-3} in a mixture of 0.005 mol•dm^{-3} Np^{4+} and 0.1 mol•dm^{-3} FHA (total FHA:Np(IV) ratio = 20:1) as Fig. 5. **Series 1**: calculated absorbance vs t plot for FHA-complexed Np(IV), obtained using eqs. (15) and (11); **Series 2**: calculated absorbance vs t plot for non-FHA-complexed Np(IV), obtained from Series 1 using eq. 8d; **Series 3**: calculated total absorbance vs t plot, obtained from sum of Series 1 & 2; **Series 4**: experimental data from Fig. 11. All theoretical plots generated using K_1 and K_D values of 2715 and 0.15.

Figure 13. Experimental and theoretical absorbance vs t plots for the Np(IV)-FHA system at [HNO_3] = 1.3 mol•dm^{-3} in a mixture of 0.005 mol•dm^{-3} Np^{4+} and 0.1 mol•dm^{-3} FHA (total FHA:Np(IV) ratio = 20:1) as Fig. 5. **Series 1**: calculated absorbance vs t plot for FHA-complexed Np(IV), obtained using eqs. (15) and (11); **Series 2**: calculated absorbance vs t plot for non-FHA-complexed Np(IV), obtained from Series 1 using eq. 8d; **Series 3**: calculated total absorbance vs t plot, obtained from sum of Series 1 & 2; **Series 4**: experimental data from Fig. 11. All theoretical plots generated using K_1 and K_D values of 2715 and 0.15.

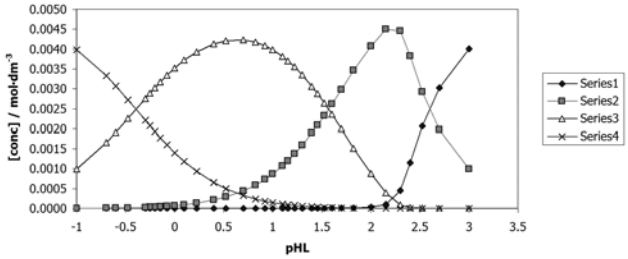

FIGURE 1

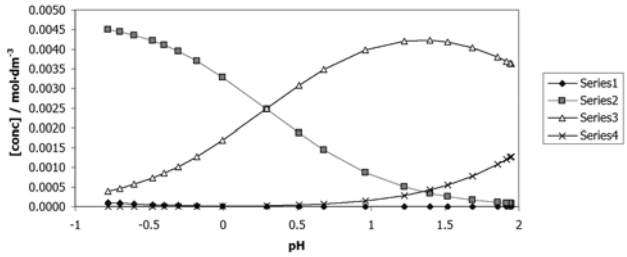

FIGURE 2

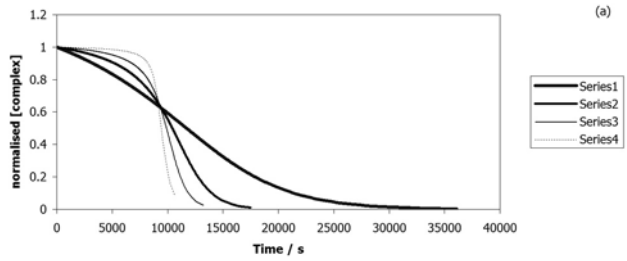

FIGURE 3a

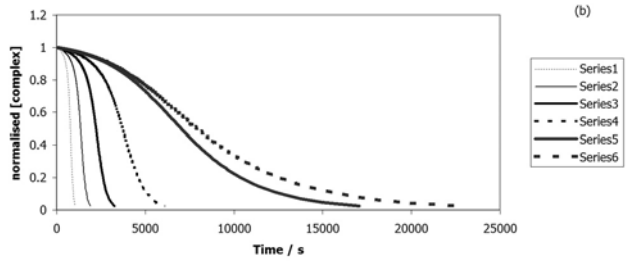

FIGURE 3b

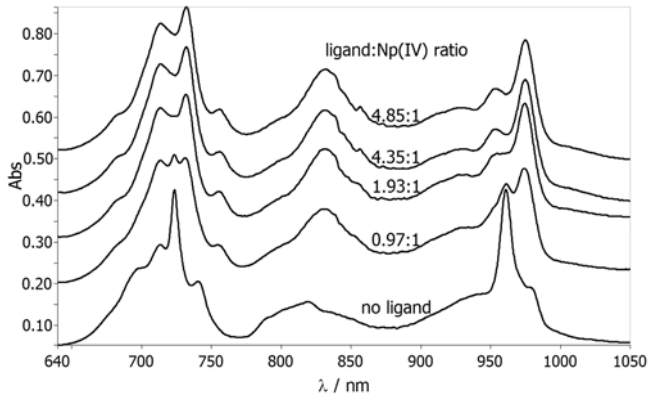

FIGURE 4

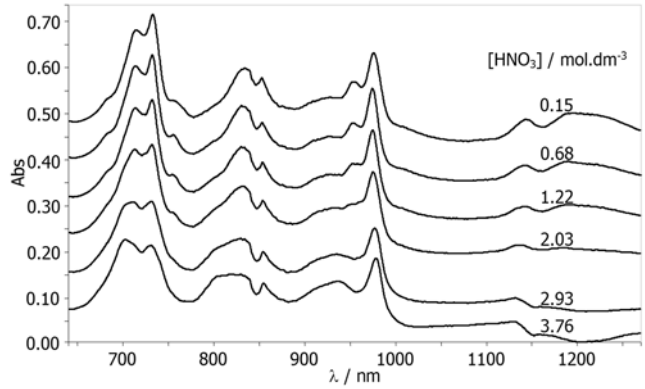

FIGURE 5

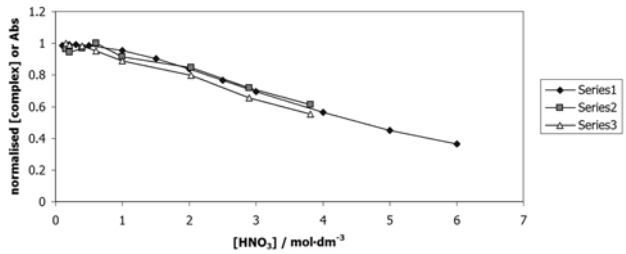

FIGURE 6

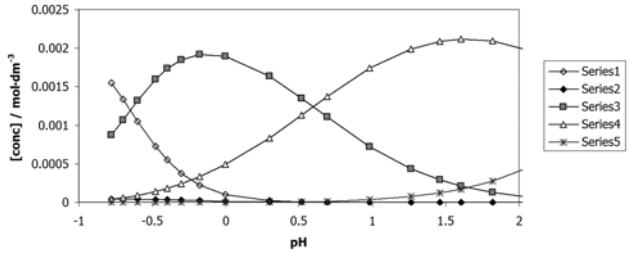

FIGURE 7

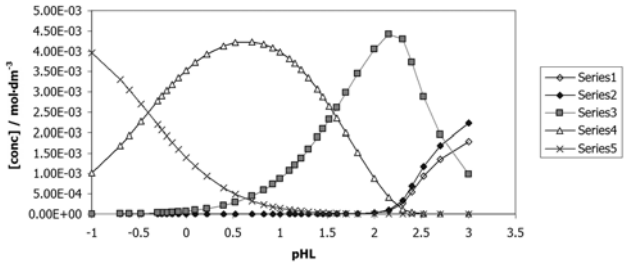

FIGURE 8

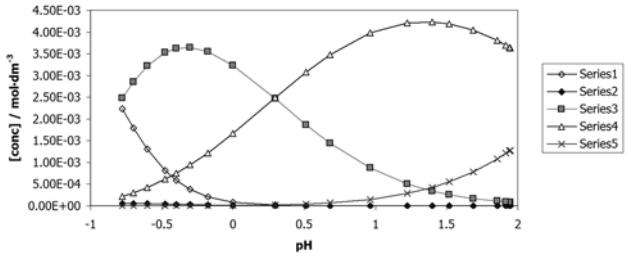

FIGURE 9

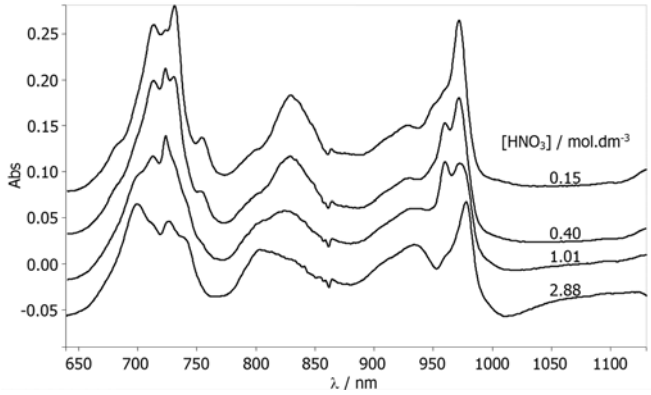

FIGURE 10

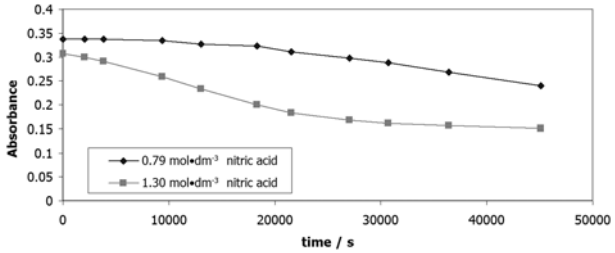

FIGURE 11

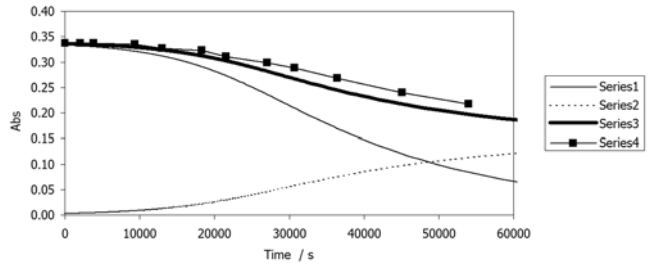

FIGURE 12

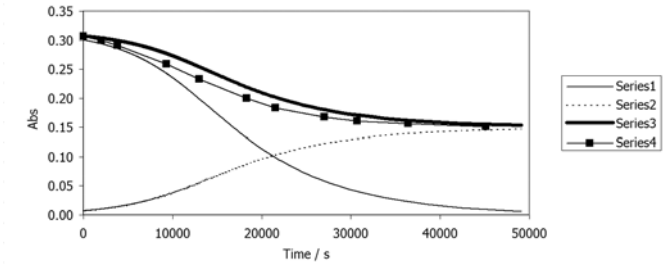

FIGURE 13